A comprehensive analysis of ^{26}Mg(^{3}H,^{2}H)^{27}Mg reaction at 36 MeV

M. Aygun[a], Z. Aygun[b], and N. Karaali[a]

[a]*Department of Physics, Bitlis Eren University, Bitlis, Turkey.*
[b]*Vocational School of Technical Sciences, Bitlis Eren University, Bitlis, Turkey.*

Received 19 December 2022; accepted 26 January 2023

The angular distribution of the ^{26}Mg(^{3}H,^{2}H)^{27}Mg reaction at 36 MeV incident energy is reanalyzed by using the distorted wave Born approximation (DWBA) method. Four forms of the optical model potentials such as temperature dependent and temperature independent density distributions, different nuclear potentials, and different nucleon-nucleon interactions are used to determine the effect on the ^{26}Mg(^{3}H,^{2}H)^{27}Mg transfer reaction of the entrance channel. These analyses display the similarities and differences of all the approaches which are discussed in this work, and provide alternative density, nuclear potential and nucleon-nucleon interactions.

Keywords: Transfer reaction; density distributions; nuclear potentials; nucleon-nucleon interactions.

DOI: https://doi.org/10.31349/RevMexFis.69.051201

1. Introduction

In a transfer reaction one or more nucleons are transferred from a projectile nucleus to a target one. Transfer reactions play an important role in understanding the natural magnesium (Mg) which has three isotopes with mass numbers 24, 25 and 26. Over the past years, deuterium-induced transfer reactions such as ^{24}Mg(d,p)^{25}Mg, ^{25}Mg(d,p)^{26}Mg and ^{26}Mg(d,p)^{27}Mg have been investigated and information about ^{25}Mg, ^{26}Mg and ^{27}Mg nuclei have been obtained. Later, tritium-induced transfer reactions such as ^{24}Mg(t,p)^{26}Mg, ^{27}Al(t,α)^{26}Mg, ^{25}Mg(t,p)^{27}Mg and ^{26}Mg(t,p)^{28}Mg have been carried out to provide further information about the Mg isotopes [1–6].

In the past, the angular distribution of ^{26}Mg(^{3}H,^{2}H)^{27}Mg transfer reaction was measured at 36 MeV [7]. K. I. Pearce *et al.* [7] analyzed the experimental data by using the distorted wave Born approximation (DWBA) method. Then, Al-Farra [8] examined the experimental data for Woods-Saxon, parity and spin-orbit interactions of the optical model based on the DWBA method. From the findings obtained, it can be seen that the results of the cross-sections should be improved. Additionally, to our knowledge few theoretical studies about the ^{26}Mg(^{3}H,^{2}H)^{27}Mg transfer reaction are available in literature. In this context, we believe that a comprehensive analysis of the ^{26}Mg(^{3}H,^{2}H)^{27}Mg transfer reaction by using different approaches will provide important information on theoretical and experimental studies which will take place in the future.

In this study, we have investigated the angular distribution of the ^{26}Mg(^{3}H,^{2}H)^{27}Mg transfer reaction at 36 MeV incident energy by using the DWBA method. For this, we have first calculated the angular distributions for five different density distributions of the ^{3}H projectile. Then, we have obtained the transfer cross-section for temperature dependent density of the ^{26}Mg target nucleus. We have also calculated the transfer cross-section for nine different proximity potentials in the entrance channel. Finally, we have obtained the transfer reaction cross-section for eleven different nucleon-nucleon (NN) interactions. We have compared the theoretical results with the experimental data, and have proposed alternative density, nuclear potential and NN interactions for the analysis of the ^{26}Mg(^{3}H,^{2}H)^{27}Mg transfer reaction.

Section 2 introduces the theory of transfer reaction channels. Section 3 and 4 present the temperature independent and temperature dependent density distributions, respectively. Section 5 and 6 give the theory of different nuclear potentials and different NN interactions, respectively. Section 7 shows the results and discussion. Section 8 exhibits the summary and conclusions.

2. Theory of transfer reaction channels

For the theoretical analysis of the ^{26}Mg(^{3}H,^{2}H)^{27}Mg transfer reaction, various nucleus-nucleus and nucleon-nucleus interactions should be considered; entrance channel (^{3}H + ^{26}Mg), exit channel (^{2}H + ^{27}Mg), core-core (^{2}H + ^{26}Mg), binding potentials (n + ^{2}H and n + ^{26}Mg). The ^{3}H projectile is assumed as the composite system ^{3}H = n + ^{2}H (see Fig. 1) in the entrance channel. Then, one n is transferred to the ^{26}Mg target, and thus it leads to the composite target-like fragment ^{27}Mg = ^{26}Mg + n in the exit channel. Generally, it can be said that the interaction potentials for the entrance and exit channels of transfer reactions are different [9]. As a result of

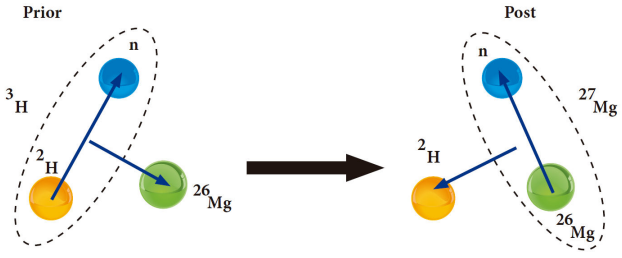

FIGURE 1. The scheme of the ^{26}Mg(^{3}H,^{2}H)^{27}Mg transfer reaction.

this, knowledge of interaction potentials is needed for the partitions. The calculation procedure associated with these potentials is described below.

2.1. Entrance channel (^{3}H + ^{26}Mg)

The potentials applied for the entrance channel, which are a dominant cause of theoretical uncertainty in the analysis of the transfer reactions, play a significant role. For this, we examine the effect of the entrance channel on the transfer cross-section by using different approaches.

The nuclear potential of the entrance channel consists of the real and the imaginary potentials. To obtain the real potential, both the optical model and the double folding model are used via the FRESCO [10] and DFPOT codes [11] which are used extensively in the analysis of various nuclear reactions [12–20]. Thus, the real part is calculated for temperature dependent and temperature independent density distributions, different nuclear potentials and different NN interactions, which all of these interactions are summarized below. The imaginary potential is in the Woods-Saxon volume form:

$$W(r) = -W_0 \left[1 + \exp\left(\frac{r - R_w}{a_w}\right)\right]^{-1}, \quad (1)$$

where W_0 is the depth, R_w is the radius, and a_w is diffuseness parameter. Additionally, the spin-orbit potential for the real part is assumed and written as

$$V_{so}(r) = -\left(\frac{\hbar}{m_\pi c}\right)^2 \left(\overrightarrow{L} \bullet \overrightarrow{S}\right) \times \frac{V_{so}}{a_{so} r} \frac{\exp\left(\frac{r-R_{so}}{a_{so}}\right)}{\left[1 + \exp(\frac{r-R_{so}}{a_{so}})\right]^2}, \quad (2)$$

where V_{so}, R_{so} and a_{so} are the depth, radius, and diffuseness parameters of the spin-orbit potential, respectively.

2.2. Exit channel (^{2}H + ^{27}Mg)

The nuclear potential of the exit channel is thought as the real, the imaginary and the spin-orbit potentials. The real part of the optical potential is written as

$$V(r) = V_0 \left[1 + \exp\left(\frac{r - R_v}{a_v}\right)\right]^{-1}. \quad (3)$$

Additionally, the spin-orbit potential for the real part is expressed as the one of the entrance channel in Eq. (2). The imaginary potential is the sum of the imaginary volume (the Woods-Saxon potential) and the imaginary surface (the surface absorption form). The imaginary volume potential is represented by Eq. (1), and the imaginary surface potential is given as follows:

$$W_D(r) = -4 a_D W_D \frac{d}{dr}\left[1 + \exp\left(\frac{r - R_D}{a_D}\right)\right]^{-1}, \quad (4)$$

where W_D is the depth, R_D is the radius, and a_D is diffuseness parameter of imaginary surface potential.

2.3. Core-Core (^{2}H + ^{26}Mg)

The core-core potential, which means the interaction between core and core nuclei, contains the real, the imaginary and the spin-orbit potentials. As a result, the nuclear potential is the same form with the potentials of the exit channel.

2.4. Binding potentials

Finally, the binding potential for the ^{26}Mg(^{3}H,^{2}H)^{27}Mg transfer reaction is composed by two parts, one for the entrance and one for the exit channels. The binding potential for the entrance potential is n + ^{2}H, and the binding potential for exit channel is n + ^{26}Mg. Only the real potential is assumed and taken as the same form with Eq. (3) with Woods-Saxon potential having standard geometry parameters r_0 = 1.25 fm and a = 0.65 fm. Its depth is determined from the binding energies.

3. ^{3}H density distributions

In our study, five different density distributions of the ^{3}H projectile have been examined, and are summarized below. However, the density distribution of the ^{26}Mg target nucleus is evaluated as

$$\rho(r) = \frac{\rho_0}{1 + \exp(\frac{r-c}{z})}, \quad (5)$$

where ρ_0, c and z parameters are 0.1695 fm^{-3}, 3.05 fm and 0.523 fm, respectively [21].

3.1. The variational Monte Carlo (VMC)

Steven *et al.* [22] reported the ^{3}H density which was obtained from the Variational Monte Carlo (VMC) calculations using the Argonne v18 (AV18) two-nucleon and Urbana X three-nucleon potentials (AV18+UX). The VMC density is taken from Ref. [23].

3.2. Gauss 1 (G1)

The G1 density is given by

$$\rho(r) = \rho_0 \exp(-r^2/\alpha^2), \quad (6)$$

where ρ_0 and α values are 0.224389 fm^{-3} and 0.557704 fm [24], respectively.

3.3. Gauss 2 (G2)

The G2 density can be written as

$$\rho(r) = \rho_0 \exp(-r^2/\alpha^2), \quad (7)$$

where ρ_0 and α values are 0.181828 fm^{-3} and 0.484741 fm [25], respectively.

3.4. Ngo-Ngo (Ngo)

The Ngo density can be formulated as [26, 27]

$$\rho_i(r) = \frac{\rho_{0i}}{1+\exp\left(\frac{r-C}{0.55}\right)}, \quad (i=n,p), \tag{8}$$

where

$$\rho_{0_{n(0p)}} = \frac{3}{4\pi}\frac{N(Z)}{A}\frac{1}{r^3_{0n(0p)}}, \quad C = R\left(1-\frac{1}{R^2}\right),$$
$$R = \frac{NR_n + ZR_p}{A}, \tag{9}$$

with

$$R_n = (1.1375 + 1.875\times10^{-4}A)A^{1/3},$$
$$R_p = 1.128A^{1/3}. \tag{10}$$

In the calculations, $\rho_{0_{n(0p)}}$ are 0.107975(0.0554451) fm^{-3}, and C are 1.02548 fm.

3.5. Schechter (S)

The parameters of the S density with the two parameter Fermi (2pF) shape can be taken as [28]

$$\rho_0 = 0.0930316 \text{ fm}^{-3},$$
$$R_0 = 1.49994 \text{ fm}, \quad a = 0.54 \text{ fm}. \tag{11}$$

4. The form of temperature dependent density

We examine temperature dependent case of the entrance channel of the ^{26}Mg(^{3}H,^{2}H)^{27}Mg reaction. We apply the 2pF density distribution for different temperatures as given below [29]

$$\rho_i(r) = \frac{\rho_{0i}(T)}{\left[1+\exp\left(\frac{r-R_{0i}(T)}{a_i(T)}\right)\right]}, \tag{12}$$

where the central density, ρ_{0i}, is written as

$$\rho_{0i}(T) = \frac{3A_i}{4\pi R^3_{0i}(T)}\left[1+\frac{\pi^2a_i^2(T)}{R^2_{0i}(T)}\right]^{-1}, \tag{13}$$

the half-density radius, $R_{0i}(T=0)$, is given by

$$R_{0i}(T=0) = 0.90106 + 0.10957A_i - 0.0013A_i^2$$
$$+ 7.71458\times10^{-6}A_i^3 - 1.62164\times10^{-8}A_i^4, \tag{14}$$

and the surface thickness parameter, $a_i(T=0)$, is parameterized as

$$a_i(T=0) = 0.34175 + 0.01234A_i - 2.1864\times10^{-4}A_i^2$$
$$+ 1.46388\times10^{-6}A_i^3 - 3.24263\times10^{-9}A_i^4. \tag{15}$$

To form the real part of the nuclear potential for different temperatures, we use temperature dependent cases of $R_{0i}(T)$ and $a_i(T)$ parameters given by [30]

$$R_{0i}(T) = R_{0i}(T=0)[1+0.0005T^2], \tag{16}$$
$$a_i(T) = a_i(T=0)[1+0.01T^2]. \tag{17}$$

5. The form of proximity potentials

The nuclear potential used in the explanation of a nuclear interaction has a very important place. Proximity model, which is established by J. Blocki *et al.* [31], is one of the most effective models in explaining the nuclear interactions. It includes a geometric factor and a universal function. Various proximity potentials which can change with the parameters such as the radius parameter, surface energy coefficient and universal function can be obtained from the literature [32–36]. As a result of these, we are looking for alternative nuclear potential(s) for the analysis of the ^{26}Mg(^{3}H,^{2}H)^{27}Mg transfer reaction.

5.1. Proximity 1977 (Prox 77)

Prox 77 potential [31, 37] is written as

$$V_N^{\text{Prox 77}}(r) = 4\pi\gamma b\overline{R}\Phi\left(\zeta = \frac{r-C_1-C_2}{b}\right) \text{ MeV}, \tag{18}$$

where

$$\overline{R} = \frac{C_1C_2}{C_1+C_2}, \quad C_i = R_i\left(1-\left[\frac{b}{R_i}\right]^2+...\right). \tag{19}$$

The effective radius, R_i, is given by

$$R_i = 1.28A_i^{1/3} - 0.76 + 0.8A_i^{-1/3}\text{fm} \quad (i=1,2). \tag{20}$$

The surface energy coefficient, γ, is assumed as

$$\gamma = \gamma_0\left(1-k_s\left[\frac{N-Z}{N+Z}\right]^2\right), \tag{21}$$

where $N(Z)$, respectively is total number of neutrons(protons), γ_0=0.9517 MeV/fm^2, and k_s=1.7826 [38]. The universal function $\Phi(\zeta)$ is in the following form

$$\Phi(\zeta) = \begin{cases} -\frac{1}{2}(\zeta-2.54)^2 \\ -0.0852(\zeta-2.54)^3, & \text{for } \zeta \le 1.2511 \\ \\ -3.437\ \exp(-\frac{\zeta}{0.75}), & \text{for } \zeta \ge 1.2511. \end{cases} \tag{22}$$

5.2. Proximity 1988 (Prox 88)

γ_0 and k_s values of Prox 88 potential are taken as 1.2496 MeV/fm^2 and 2.3, respectively [39]. The other parameters of Prox 88 are the same as Prox 77.

5.3. Broglia and Winther 1991 (BW 91)

BW 91 potential [39] is assumed as [40]

$$V_N^{BW\,91}(r) = -\frac{V_0}{\left[1+\exp\,\left(\frac{r-R_0}{a}\right)\right]}\text{MeV}, \qquad (23)$$

where

$$V_0 = 16\pi\frac{R_1R_2}{R_1+R_2}\gamma a, \quad a = 0.63\,\text{fm}, \qquad (24)$$

and

$$R_0 = R_1 + R_2 + 0.29,$$
$$R_i = 1.233A_i^{1/3} - 0.98A_i^{-1/3} \;\; (i=1,2), \qquad (25)$$

with γ is

$$\gamma = \gamma_0\left(1 - k_s\left[\frac{N_p - Z_p}{A_p}\right]\left(\frac{N_t - Z_t}{A_t}\right]\right). \qquad (26)$$

γ_0 and k_s are 0.95 MeV/fm^2 and 1.8, respectively.

5.4. Akyüz-Winther (AW 95)

The only difference between AW 95 and BW 91 potentials [40, 41] is

$$a = \left(\frac{1}{1.17(1+0.53(A_1^{-1/3}+A_2^{-1/3}))}\right)\text{fm}, \qquad (27)$$

and

$$R_0 = R_1 + R_2, \quad R_i = 1.2A_i^{1/3} - 0.09 \;\; (i=1,2). \qquad (28)$$

5.5. Bass 1973 (Bass 73)

Bass 73 potential [42, 43] can be written as [37]

$$V_N^{\text{Bass}\,73}(r) = -\frac{da_sA_1^{1/3}A_2^{1/3}}{R_{12}} \times \exp\left(-\frac{r-R_{12}}{d}\right) \;\; \text{MeV}, \qquad (29)$$

where

$$R_{12} = 1.07\left(A_1^{1/3}+A_2^{1/3}\right), \quad d = 1.35\,\text{fm},$$
$$\text{and} \;\; a_s = 17 \;\; \text{MeV}. \qquad (30)$$

5.6. Bass 1977 (Bass 77)

Bass 77 potential [44] is assumed as [40]

$$V_N^{Bass\,77}(s) = -\frac{R_1R_2}{R_1+R_2} \times \phi(s = r - R_1 - R_2) \;\; \text{MeV}, \qquad (31)$$

where

$$R_i = 1.16A_i^{1/3} - 1.39A_i^{-1/3} \;\; (i=1,2), \qquad (32)$$

$$\phi(s) = \left(A\exp\left[\frac{s}{d_1}\right] + B\,\exp\left[\frac{s}{d_2}\right]\right)^{-1}, \qquad (33)$$

with $A = 0.030\,\text{MeV}^{-1}$ fm, $B = 0.0061\,\text{MeV}^{-1}$ fm, $d_1 = 3.30$ fm, and $d_2 = 0.65$ fm.

5.7. Bass 1980 (Bass 80)

The only difference between Bass 80 and Bass 77 potentials is the function $\phi(s = r - R_1 - R_2)$, and can be given by [39, 40]

$$\phi(s) = \left(0.033\;\exp\left[\frac{s}{3.5}\right] + 0.007\;\exp\left[\frac{s}{0.65}\right]\right)^{-1}, \qquad (34)$$

and

$$R_i = R_s\left(1 - \frac{0.98}{R_s^2}\right),$$
$$R_s = 1.28A_i^{1/3} - 0.76 + 0.8A_i^{-1/3}\,\text{fm} \;\; (i=1,2). \qquad (35)$$

5.8. Christensen and Winther 1976 (CW 76)

CW 76 potential [45] can be exhibited by [37]

$$V_N^{CW\,76}(r) = -50\frac{R_1R_2}{R_1+R_2} \times \phi(s = r - R_1 - R_2) \;\; \text{MeV}, \qquad (36)$$

where

$$R_i = 1.233A_i^{1/3} - 0.978A_i^{-1/3}\,\text{fm} \quad (i=1,2), \qquad (37)$$

$$\phi(s) = \exp\left(-\frac{r-R_1-R_2}{0.63}\right). \qquad (38)$$

5.9. Ngô 1980 (Ngo 80)

Ngo 80 potential can be parameterized by [26]

$$V_N^{Ngo\,88}(r) = \overline{R}\phi(r - \xi_1 - \xi_2) \;\; \text{MeV}, \qquad (39)$$

$$\overline{R} = \frac{\xi_1\xi_2}{\xi_1+\xi_2},$$
$$\xi_i = R_i\left(1 - \left[\frac{b}{R_i}\right]^2 + ...\right), \qquad (40)$$

$$R_i = \frac{NR_{ni} + ZR_{pi}}{A_i} \quad (i=1,2), \qquad (41)$$

$$R_{pi} = r_{0pi}A_i^{1/3}, \quad R_{ni} = r_{0ni}A_i^{1/3}, \qquad (42)$$

$$r_{0pi} = 1.128 \;\; \text{fm},$$
$$r_{0ni} = 1.1375 + 1.875\text{x}10^{-4}A_i \;\; \text{fm}. \qquad (43)$$

The universal function $\phi(\varsigma = r - \xi_1 - \xi_2)$ (in MeV/fm) is written as

$$\Phi(\varsigma) = \begin{cases} -33 + 5.4(\varsigma - \varsigma_0)^2, & \text{for} \quad \varsigma < \varsigma_0 \\ -33 \ \exp[-\frac{1}{5}(\varsigma - \varsigma_0)^2] & \text{for} \quad \varsigma \geq \varsigma_0 \\ \varsigma_0 = -1.6 \ \text{fm} \end{cases} . \quad (44)$$

6. The form of microscopic NN interactions

The double folding model is a very effective model in obtaining the real part of the nuclear potential. It requests the NN interaction and density distributions of projectile and target nuclei. Therefore, the optimal NN interaction should be determined for the analyzed system. In this context, we examine the effect on the cross-section of the ^{26}Mg(^{3}H,^{2}H)^{27}Mg transfer reaction of eleven different NN interactions which consist of the HS [49], Z [49], W [49], L1 [49], L2 [49], L3 [49], TS [50], NL1 [49], NL2 [49], NL3 [51] and NL3* [52]. As a result of this, we can discuss the similarities and differences of various NN interactions examined in our study.

The effective NN interaction can be formulated as the sum of scalar and vector parts of the single meson fields given by [46–48]

$$\nu_{NN}(r) = \frac{g_w^2}{4\pi}\frac{e^{-m_w r}}{r} + \frac{g_\rho^2}{4\pi}\frac{e^{-m_\rho r}}{r} - \frac{g_\sigma^2}{4\pi}\frac{e^{-m_\sigma r}}{r} + \frac{g_2^2}{4\pi} r e^{-2m_\sigma r} + \frac{g_3^2}{4\pi} r \frac{e^{-3m_\sigma r}}{r}, \quad (45)$$

where g_w, g_ρ and g_σ are the coupling constants, and m_w, m_ρ and m_σ are the masses for w, ρ and σ mesons, respectively. If the single nucleon exchange effect is added, the equation (45) becomes

$$\nu_{NN}(r) = \frac{g_w^2}{4\pi}\frac{e^{-m_w r}}{r} + \frac{g_\rho^2}{4\pi}\frac{e^{-m_\rho r}}{r} - \frac{g_\sigma^2}{4\pi}\frac{e^{-m_\sigma r}}{r} + \frac{g_2^2}{4\pi} r e^{-2m_\sigma r} + \frac{g_3^2}{4\pi} r \frac{e^{-3m_\sigma r}}{r} + J_{00}(E)\delta(r). \quad (46)$$

The exchange term is written as

$$J_{00}(E) = -276 \left(1 - 0.005 \frac{E_{\text{Lab}}}{A_p}\right) \text{MeV fm}^3, \quad (47)$$

where E_{Lab} and A_p are the incident energy and mass number of the projectile, respectively. The parameters of all the NN interactions are listed in Table I.

7. Results and discussion

The theoretical calculations of the transfer cross-section of ^{26}Mg(^{3}H,^{2}H)^{27}Mg reaction at 36 MeV consist of four different stages. We have first used the parameters reported in Ref. [7] as starting values of the optical potential parameters of the entrance channel. The optical potential parameters for the exit channel and core-core channel come from global deuteron potentials [53]. Then, we have performed the pa-

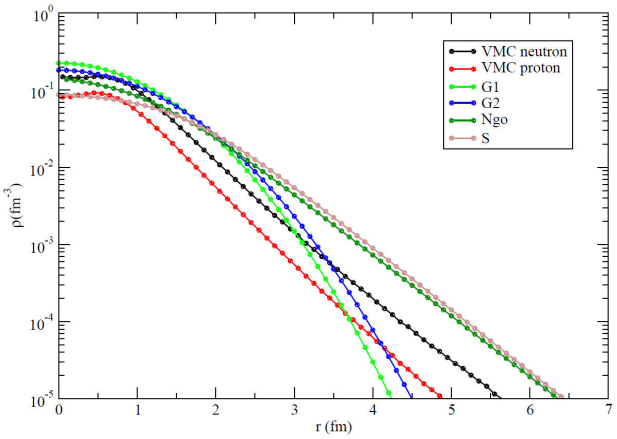

FIGURE 2. The changes with the distance of VMC, G1, G2, Ngo and S density distributions in logarithmic scale.

TABLE I. The values of the m_σ (in MeV), m_w (in MeV), m_ρ (in MeV), g_σ, g_w, g_ρ, g_2 and g_3 parameters of eleven different NN interactions including HS, Z, W, L1, L2, L3, TS, NL1, NL2, NL3, and NL3* interactions.

Parameter	m_σ	m_w	m_ρ	g_σ	g_w	g_ρ	g_2	g_3
HS	520	783	770	10.4814	13.8144	8.08488	-	-
Z	551.31	780	763	11.1933	13.8256	10.8883	-	-
W	550	783	-	9.57371	11.6724	-	-	-
L1	550	783	-	10.2999	12.5999	-	-	-
L2	546.940	780	763	11.3972	14.2478	-	-	-
L3	492.260	780	763	10.6920	14.8705	-	-	-
TS	597.6	783	770	11.2060	12.7200	2.78	-	-
NL1	492.250	795.359	763	10.1377	13.2846	9.95145	-12.1724	-36.2646
NL2	504.890	780	763	9.11122	11.4928	10.7732	-2.30404	13.7844
NL3	508.194	782.501	763	10.2170	12.8680	4.474	-10.4310	-28.885
NL3*	502.5742	782.6	763	10.0944	12.8065	4.5748	-10.8093	-30.1486

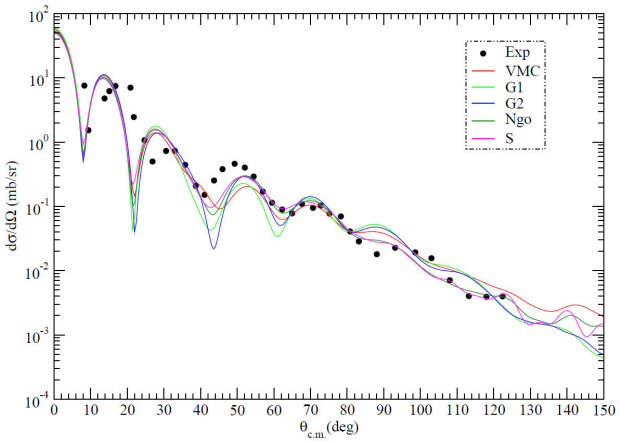

FIGURE 3. The cross-sections of the ^{26}Mg(^{3}H,^{2}H)^{27}Mg transfer reaction calculated by using VMC, G1, G2, Ngo and S densities in comparison with the experimental data at 36 MeV [54].

rameter search in order to obtain the best-fit with the experimental data. In order to reduce ambiguity in fitting procedure, the geometrical parameters (radius, diffuseness) are usually fixed to average values, and then the potential depths (V_0, W_v, W_d, and V_{so}) are adjusted to improve the fit quality. In all the calculations, r_w=1.65 fm, a_w=0.74 fm, r_{so}=1.36 fm and a_{so}=1.18 fm for ^{3}H + ^{26}Mg channel, r_v=1.17 fm, a_v=0.77 fm, r_w=r_d=1.325 fm, a_w=a_d=0.74 fm, r_{so}=1.07 fm and a_{so}=0.66 fm for ^{2}H + ^{27}Mg channel, and r_v=1.17 fm, a_v=0.77 fm, r_w=r_d=1.325 fm, a_w=a_d=0.737 fm, r_{so}=1.07 fm and a_{so}=0.66 fm for ^{2}H + ^{26}Mg channel. In the folding model calculations, we have also fixed the renormalisation factor (N_r) as one and have not changed its default value (≈ 1.0). Thus, we have eliminated the effect of the N_r value on the cross-section calculations.

7.1. Analysis for different densities

We have examined the effect of different density distributions of the ^{3}H projectile in the entrance channel. We have used five type densities in the calculations which consist of VMC, G1, G2, Ngo and S. We have obtained the real potentials within the scope of the double folding model for these densities. In this context, we display the radial changes of the density distributions in Fig. 2.

We have calculated the transfer cross-section of ^{26}Mg(^{3}H,^{2}H)^{27}Mg reaction at 36 MeV, and compare the results together with the experimental data in Fig. 3. We have also listed the optical potential parameters used in obtaining the theoretical results in Table II. The results are very similar to each other at small angles although there are differences in the results at forward angles. The behaviors of Ngo and S results are close to each other as well as those of G1 and G2. The theoretical results are in good agreement with the data. Additionally, the results with the Ngo and S densities are better than the results of the other densities in agreement with the data. Thus, we can say that the Ngo and S densities can be especially used as alternative density distributions for the analysis of the ^{26}Mg(^{3}H,^{2}H)^{27}Mg transfer reaction.

7.2. Analysis for temperature dependent density

Here, we have examined the effect on the reaction cross-section of temperature dependent density of the ^{26}Mg target nucleus in the entrance channel. We have used the 2pF density for temperature dependent (T = 1, 2, 3, 4, 5, 6 and 7 MeV) and temperature independent ($T = 0$ MeV) cases of the ^{26}Mg nucleus. We have calculated the density distributions based on the temperature of ^{26}Mg, and show the radial changes of the densities in Fig. 4. We observe

TABLE II. The optical potential parameters of the entrance channel, exit channel and core-core potentials used in the calculations of different density distributions.

Potential	VMC	G1	G2	Ngo	S
		^{3}H + ^{26}Mg			
W_v (MeV)	13.0	13.0	14.0	14.0	14.0
V_{so} (MeV)	1.70	1.00	1.00	1.00	2.70
		^{2}H + ^{27}Mg			
V_0 (MeV)	69.0	72.0	69.0	69.0	69.0
W_v (MeV)	2.40	2.30	1.40	2.40	2.40
W_d (MeV)	11.0	11.0	11.0	11.0	11.0
V_{so} (MeV)	3.30	1.30	1.30	3.30	3.30
		^{2}H + ^{26}Mg			
V_0 (MeV)	86.2	84.0	84.0	86.2	86.2
W_v (MeV)	4.60	1.60	1.60	1.60	1.60
W_d (MeV)	5.34	5.54	5.54	5.54	5.54
V_{so} (MeV)	6.30	6.30	6.30	6.30	6.30

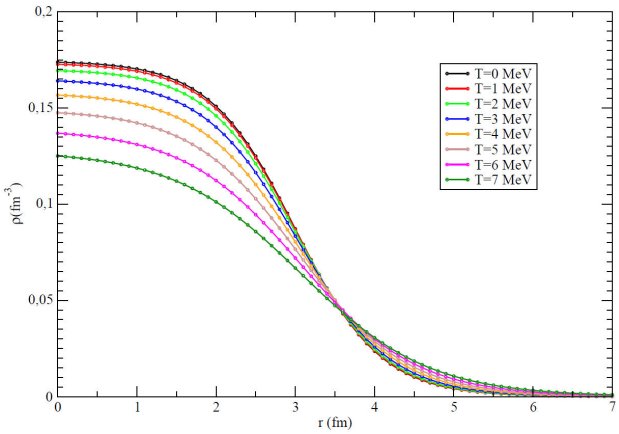

FIGURE 4. The changes with the distance of the density distributions of the ^{26}Mg nucleus for T = 0, 1, 2, 3, 4, 5, 6 and 7 MeV in linear scale.

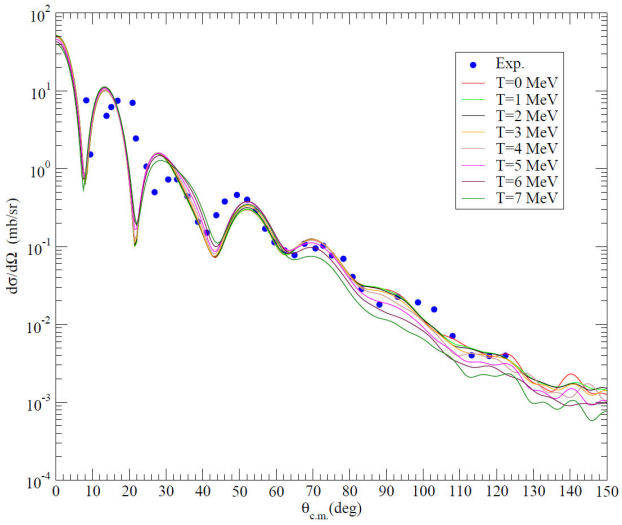

FIGURE 5. The cross-sections of the ^{26}Mg(^{3}H,^{2}H)^{27}Mg transfer reaction for the densities of the ^{26}Mg nucleus in comparison with the experimental data [54] at $T = 0$, 1, 2, 3, 4, 5, 6 and 7 MeV.

TABLE III. The optical potential parameters of the entrance channel, exit channel and core-core potentials used in the analysis with temperature dependent density.

Channel	V_0 (MeV)	W_v (MeV)	W_d (MeV)	V_{so} (MeV)
^{3}H + ^{26}Mg	–	14.0	–	1.00
^{2}H + ^{27}Mg	69.0	2.40	11.0	3.30
^{2}H + ^{26}Mg	86.2	1.60	5.54	6.30

that the ^{26}Mg densities change with varying of the temperature. We can say that the densities in the center decrease with increasing of the temperature, and the tailing of densities increase with increasing temperature.

Then we have calculated the cross-section of the transfer reaction for the densities calculated at $T = 1$, 2, 3, 4, 5, 6 and 7 MeV. We compare the theoretical results and the experimental data in Fig. 5. We given the optical potential parameters for all the channels in Table III. While determining the optical model parameters, we have first searched the potential parameters providing good agreement results with the experimental data for $T = 0$ MeV case. For $T = 1$, 2, 3, 4, 5, 6 and 7 MeV calculations, we have applied without changing the potential parameters used in $T = 0$ MeV case. The aim of this is to see only the temperature dependent effect without changing any potential parameter. We have observed that the results from $T = 1$ MeV to $T = 7$ MeV are different from each other. As a consequence, we can deduce that the temperature changes the cross section somewhat. Additionally, the changes in the cross section values are very small and the oscillation pattern of the angular distribution is not a function of T.

7.3. Analysis for different nuclear potentials

In the present study, we have also examined the effect on the cross-section of the ^{26}Mg(^{3}H,^{2}H)^{27}Mg transfer reaction of nine different potentials which consist of Prox 77, Prox 88, AW 95, Bass 73, Bass 77, Bass 80, BW 91, CW 76 and Ngo 80 for the entrance channel. In this respect, we demonstrate the distance dependent variations of the potentials in Fig. 6.

We have obtained the transfer cross-sections for the nuclear potentials, and compare each result separately in Figs. 7 and 8. We have also listed the optical potential parameters for all the channels in Table IV. We have observed that the behaviors of the results with the Prox 77 and Ngo potentials are very close to each other while the behavior of the Bass 77 and Bass 80 results is generally similar. The other potentials generally differ from each other, especially at forward angles. CW76 and BW91 are not clearly working properly at forward angles. We have realized that the Prox 77, Prox 88, Bass 77, Bass 80 and Ngo 80 results are in good agreement with the experimental data, and are slightly better than the results of the other potentials.

7.4. Analysis for different NN interactions

Finally we have investigated the effect on the transfer cross-section of eleven kind NN interactions which consist of HS, Z, W, L1, L2, L3, TS, NL1, NL2, NL3 and NL3*. We have produced the real potentials of the entrance channel for these NN interactions. We show the radial changes of all the NN interactions in Fig. 9. We observe that the behaviors of the NN interactions are similar to each other. However, we have noticed that the shallowest potential is for NL2, and the deepest potential is for L2.

We display the transfer cross-sections together with the experimental data in Fig. 10, and list the optical potential parameters of all the NN interactions in Table V. We observe that the results with different NN interaction potentials show similar and differences. We have seen that the behaviors of the results with the Z, W and TS interactions are close to each other. We have realized that the

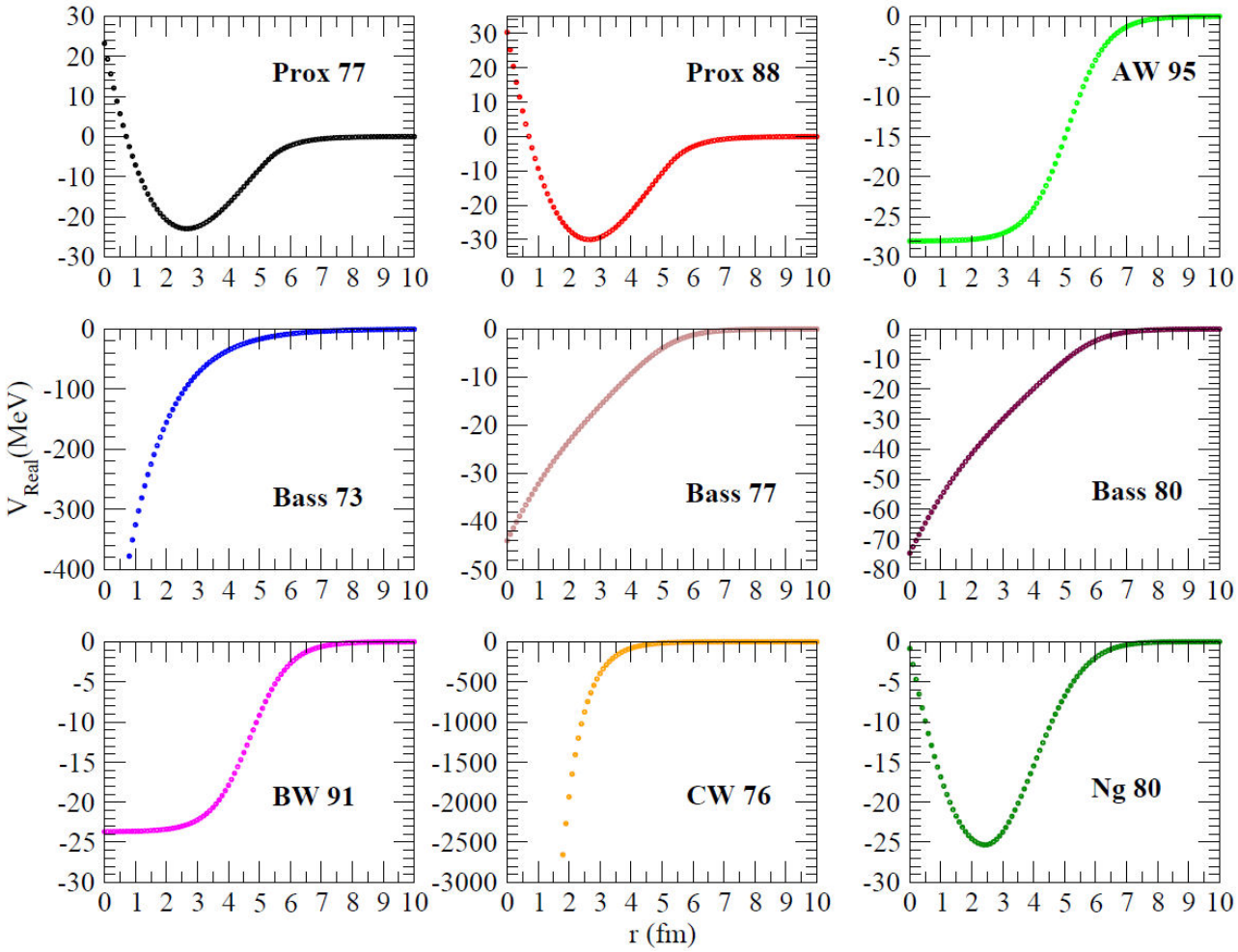

FIGURE 6. Distance-dependent changes of Prox 77, Prox 88, AW 95, Bass 73, Bass 77, Bass 80, BW 91, CW 76 and Ngo 80 potentials.

TABLE IV. The optical potential parameters of the entrance channel, exit channel and core-core potentials used in the calculations of different nuclear potentials.

Potential	Prox 77	Prox 88	AW 95	Bass 73	Bass 77	Bass 80	BW 91	CW 76	Ngo 80
				^{3}H + ^{26}Mg					
W_v (MeV)	11.2	12.0	12.0	11.0	9.50	11.5	12.5	12.1	11.1
V_{so} (MeV)	2.00	3.00	1.00	1.00	4.00	3.00	1.00	1.00	2.20
				^{2}H + ^{27}Mg					
V_0 (MeV)	70.0	73.5	72.0	70.3	72.0	72.0	72.0	70.0	70.0
W_v (MeV)	1.90	2.20	2.30	2.10	1.30	1.30	1.30	2.00	1.90
W_d (MeV)	10.8	10.8	11.0	11.0	11.0	11.0	11.0	11.0	10.8
V_{so} (MeV)	2.30	2.60	1.30	1.30	1.30	1.30	1.30	2.30	2.30
				^{2}H + ^{26}Mg					
V_0 (MeV)	90.0	94.0	86.0	86.0	88.0	87.0	88.0	90.0	90.0
W_v (MeV)	1.60	2.90	5.60	4.60	4.60	3.60	4.60	4.60	3.60
W_d (MeV)	2.70	2.70	4.54	4.10	4.70	4.70	3.70	2.70	2.70
V_{so} (MeV)	6.30	6.30	6.30	6.30	6.30	6.30	6.30	6.30	6.30

TABLE V. The optical potential parameters of the entrance channel, exit channel and core-core potentials used in the calculations of different NN interactions.

Potential	HS	Z	W	L1	L2	L3	TS	NL1	NL2	NL3	NL3*
				^{3}H + ^{26}Mg							
W_v (MeV)	10.0	25.0	21.0	10.0	9.50	9.00	21.0	26.0	21.0	24.0	24.0
V_{so} (MeV)	2.70	4.60	1.00	2.70	1.70	1.70	1.00	1.00	1.00	1.00	1.00
				^{2}H + ^{27}Mg							
V_0 (MeV)	72.0	65.7	62.5	62.0	68.0	68.0	62.5	68.0	63.5	61.5	64.5
W_v (MeV)	2.30	1.30	1.20	5.30	5.30	1.60	1.20	1.60	1.20	1.20	1.20
W_d (MeV)	11.0	5.70	5.70	9.00	9.00	9.00	5.70	6.50	6.50	6.50	6.50
V_{so} (MeV)	2.10	1.00	1.00	9.00	9.00	9.00	1.00	3.00	1.00	1.00	1.00
				^{2}H + ^{26}Mg							
V_0 (MeV)	84.7	80.7	80.7	94.7	94.7	94.7	83.7	92.7	92.7	88.7	88.7
W_v (MeV)	7.00	8.00	2.00	1.00	3.00	3.00	2.00	3.00	1.00	1.00	2.00
W_d (MeV)	3.00	4.60	4.60	1.00	1.20	1.20	4.60	6.40	6.40	4.40	3.60
V_{so} (MeV)	6.30	6.30	6.30	6.30	6.30	6.30	6.30	6.30	6.30	6.30	6.30

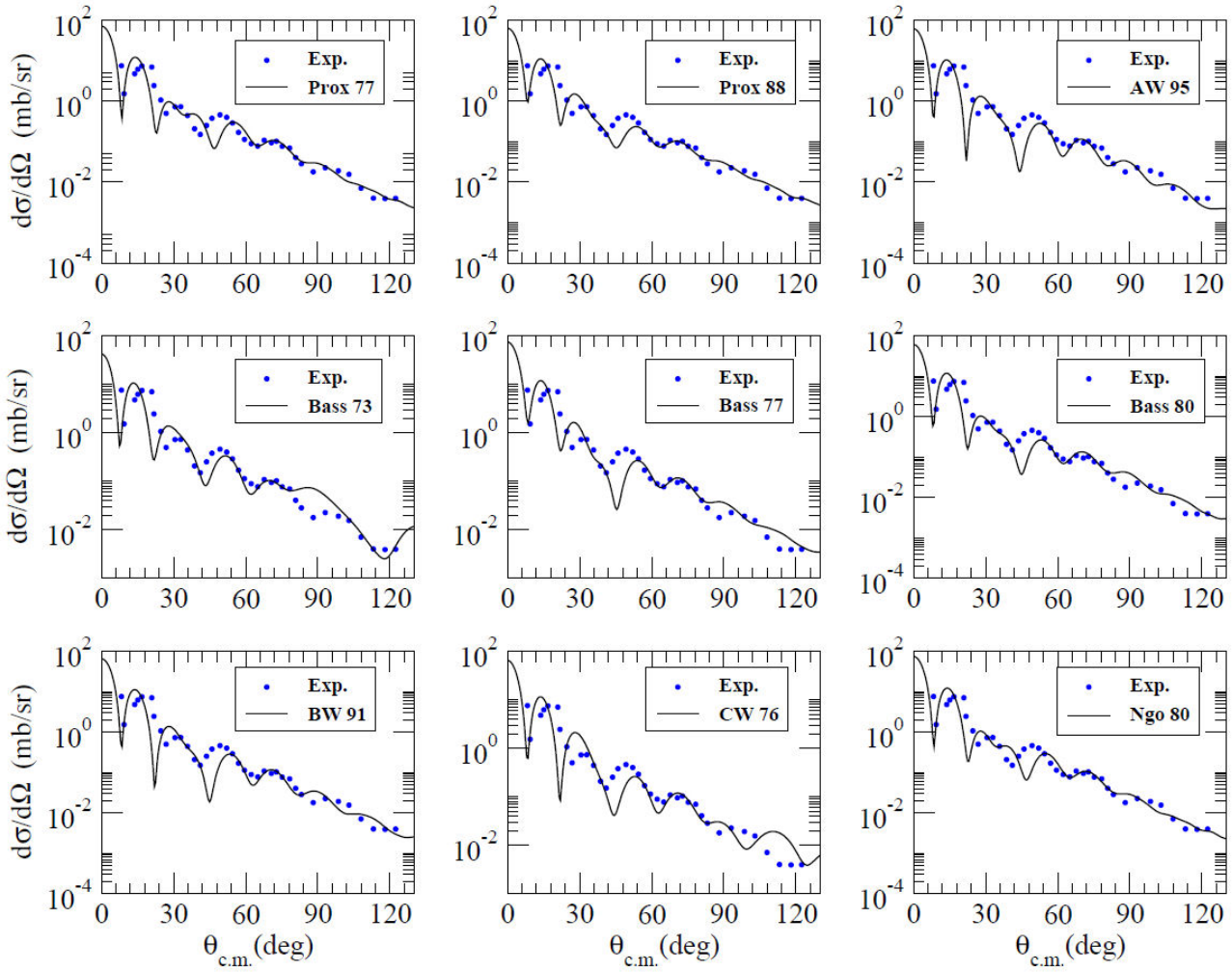

FIGURE 7. The cross-sections of the ^{26}Mg(^{3}H,^{2}H)^{27}Mg transfer reaction calculated by using Prox 77, Prox 88, AW 95, Bass 73, Bass 77, Bass 80, BW 91, CW 76 and Ngo 80 potentials in comparison with the experimental data [54].

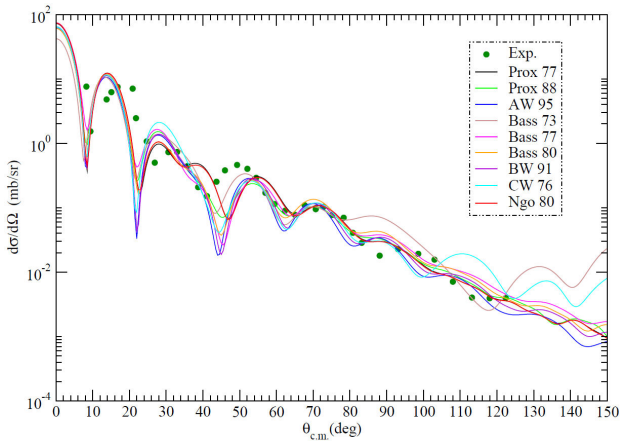

FIGURE 8. Comparison of both the experimental data and the cross-sections of the ^{26}Mg(^{3}H,^{2}H)^{27}Mg transfer reaction calculated by using Prox 77, Prox 88, AW 95, Bass 73, Bass 77, Bass 80, BW 91, CW 76 and Ngo 80 potentials.

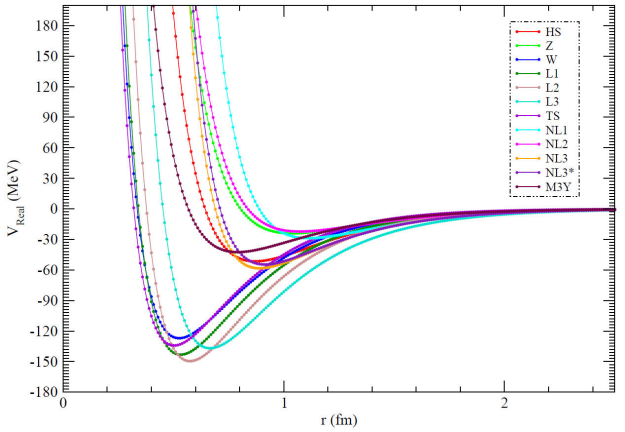

FIGURE 9. Distance-dependent changes of the HS, Z, W, L1, L2, L3, TS, NL1, NL2, NL3, NL3* and M3Y interactions.

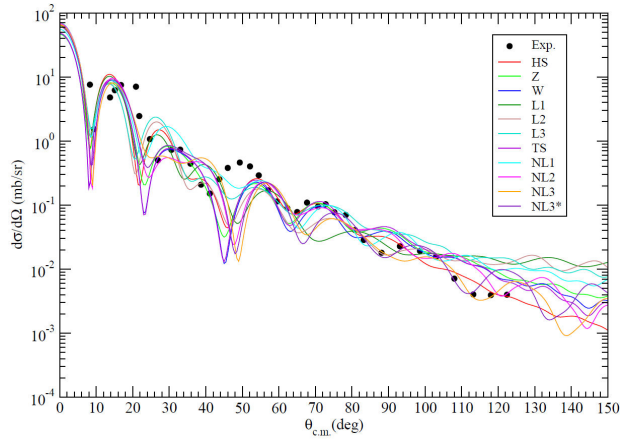

FIGURE 10. The cross-sections of the ^{26}Mg(^{3}H,^{2}H)^{27}Mg transfer reaction calculated by using the HS, Z, W, L1, L2, L3, TS, NL1, NL2, NL3 and NL3* interactions in comparison with the experimental data [54].

L1, L2, L3 and NL1 results are generally far from describing the experimental data. Additionally, we can express that the results with the HS, Z, W and TS interactions are better than the results of the other NN interactions.

8. Summary and conclusions

We have carried out a comprehensive review of the ^{26}Mg(^{3}H,^{2}H)^{27}Mg transfer reaction at 36 MeV incident energy by using temperature dependent and temperature independent densities, different nuclear potentials, and different NN interactions. We have calculated the transfer cross-sections within the code FRESCO based on the DWBA method. We have proposed alternative density distributions which can be used in the analysis of the ^{26}Mg(^{3}H,^{2}H)^{27}Mg transfer reaction. We have observed that the temperature changes the transfer cross-section somewhat. We can also say that the changes in the cross section values are very small and the oscillation pattern of the angular distribution is not a function of T. Then, we have displayed that Prox 77, Prox 88, Bass 77, Bass 80 and Ngo 80 can be used as alternative potentials in analyzing the ^{26}Mg(^{3}H,^{2}H)^{27}Mg transfer reaction. Also, we have shown that HS, Z, W, and TS can be alternative NN interactions to the M3Y interaction for the analysis of ^{26}Mg(^{3}H,^{2}H)^{27}Mg transfer reaction. Finally, we have observed that the results of alternative density, nuclear potential and NN interactions suggested with this study are better than the results obtained by both Farra [8] and Timofeyuk [55] when we have compared our results with the literature. We believe that it would be interesting and useful to implement these approaches to another transfer reactions.

Acknowledgements

The authors thank the referee for valuable discussion and comments. The authors are also very grateful to the Scientific and Technological Research Council of Türkiye (TUBITAK) for the financial support (Project Number: 122F275).

1. J. R. Holt and T. N. Marsham, *An Investigation of (d,p) Stripping Reactions II: Results for the Isotopes of Magnesium*, Proc. Phys. Soc. A **66** (1953) 258. https://doi.org/10.1088/0370-1298/66/3/308.
2. S. Hinds, H. Marchant and R. Middleton, *The Energy Levels of the Magnesium Isotopes of Mass 25 to 28*, Proc. Phys. Soc. **78** (1961) 473. https://doi.org/10.1088/0370-1328/78/4/301.
3. S. Hinds, R. Middleton and G. Parry, *An Investigation of the Reactions ^{24}Mg(d,p)^{25}Mg and ^{26}Mg(d,p)^{27}Mg by Magnetic Analysis*, Proc. Phys. Soc. **71** (1958) 49. https://doi.org/10.1088/0370-1328/71/1/307.
4. P. M. Endt, H. A. Enge, J. Haffner and W. W. Buechner, *Excited States of Mg^{25} from the Al^{27}(d,α)Mg^{25} and Mg^{24}(d,p)Mg^{25} Reactions*, Phys. Rev. **87** (1952) 27. https://doi.org/10.1103/PhysRev.87.27.
5. P. M. Endt, J. W. Haffner and D. M. Van Patter, *Magnetic Analysis of the Mg^{25}(d,p)Mg^{26}, Mg^{26}(d,p)Mg^{27}, and Mg^{25}(d,α)Na^{23} Reactions*, Phys. Rev. **86** (1952) 518. https://doi.org/10.1103/PhysRev.86.518.
6. D. G. McNeel, A. H. Wuosmaa, S. A. Kuvin, J. Smith, B. B. Back, J. Chen, C. R. Hoffman, B. P. Kay, G. L. Wilson, D. K. Sharp, R. M. Clark, H. L. Crawford, P. Fallon and A. O. Macchiavelli, *Configuration mixing in ^{28}Mg and the ^{26}Mg(t,p)^{28}Mg reaction*, Phys. Rev. C **103** (2021) 064320. https://doi.org/10.1103/PhysRevC.103.064320.
7. K. I. Pearce, N. M. Clarke, R. J. Griffiths, P. J. Simmonds, D. Barker, J. B. A. England, M. C. Mannion and C. A. Ogilvie, *36 MeV triton inelastic scattering and one-nucleon transfer reactions*, Nucl. Phys. A **467** (1987) 215-239. https://doi.org/10.1016/0375-9474(87)90527-6.
8. A. K. A. R. Al-Farra, *Analysis of One-Nucleon Transfer Cross-Sections*, Turk. J. Phys. **28** (2004) 169-174.
9. N. Burtebayev, Sh. Hamada, Awad A. Ibraheem, K. Rusek, M. Wolinska-Cichocka, J. Burtebayev, N. Amangeldi, Maulen Nassurlla, Marzhan Nassurlla and A. Sabidolda, *Effect of the Transfer Reactions for ^{16}O+^{10}B Elastic Scattering*, Acta Phys. Pol. B **50** (2019) 1423. https://doi.org/10.5506/APhysPolB.50.1423.
10. I. J. Thompson, *Coupled reaction channels calculations in nuclear physics*, Comp. Phys. Rep. **7** (1988) 167. https://doi.org/10.1016/0167-7977(88)90005-6.
11. J. Cook, *DFPOT - A program for the calculation of double folded potentials*, Commun. Comput. Phys. **25** (1982) 125-139. https://doi.org/10.1016/0010-4655(82)90029-7.
12. M. Aygun and H. Cin, *A comprehensive analysis of ^{19}F + ^{9}Be, ^{12}C, ^{16}O, ^{19}F, ^{27}Al, ^{28,30}Si, ^{40}Ca, ^{54,56}Fe, ^{208}Pb, ^{232}Th fusion reactions*, Rev. Mex. Fis. **68** (2022) 1-11. https://doi.org/10.31349/RevMexFis.68.031202.
13. M. Aygun, *An investigation of alpha-transfer reaction ^{28}Si(^{20}Ne,^{16}O)^{32}S*, Rev. Mex. Fis. **67** (2021) 1-7. https://doi.org/10.31349/RevMexFis.67.041201.
14. T. Ulucay and M. Aygun, *A comprehensive description of elastic scattering angular distributions for eight different density distribution of ^{32}S nucleus*, Rev. Mex. Fis. **66** (2020) 336-343. https://doi.org/10.31349/RevMexFis.66.336.
15. M. Aygun and Z. Aygun, *A comprehensive analysis of ^{9}Li + ^{70}Zn fusion cross section by using proximity potentials, temperature dependent density distributions and nuclear potentials*, Rev. Mex. Fis. **65** (2019) 573-582. https://doi.org/10.31349/RevMexFis.65.573.
16. M. Aygun and Z. Aygun, *Microscopic analysis of elastic scattering cross sections for different densities of ^{8}Li nucleus on light, medium and heavy mass targets*, Rev. Mex. Fis. **65** (2019) 404-411. https://doi.org/10.31349/RevMexFis.65.404.
17. M. Aygun, *A comprehensive study on the internal structure and thedensity distribution of ^{12}Be*, Rev. Mex. Fis. **62** (2016) 336-343.
18. M. Aygun, O. Kocadag and Y. Sahin, *A comprehensive analysis of ^{19}F + ^{9}Be, ^{12}C, ^{16}O, ^{19}F, ^{27}Al, ^{28,30}Si, ^{40}Ca, ^{54,56}Fe, ^{208}Pb, ^{232}Th fusion reactions*, Rev. Mex. Fis. **61** (2015) 414-420.
19. M. Aygun, *A Microscopic Analysis of Elastic Scattering of ^{8}Li Nucleus on Different Target Nuclei*, Acta Phys. Pol. B **45** (2014) 1875. https://doi.org/10.5506/APhysPolB.45.1875.
20. M. Aygun, *Reanalysis of elastic scattering of ^{6}Li + ^{209}Bi reaction using a new density distribution of ^{6}Li nucleus*, Commun. Theor. Phys. **60** (2013) 69-72. https://doi.org/10.1088/0253-6102/60/1/09.
21. S. Hossain, M. N. A. Abdullah, Md Z. Rahman, A. K. Basak and F. B. Malik, *Non-monotonic potentials for ^{6}Li elastic scattering at 88 MeV*, Phys. Scr. **87** (2013) 015201. https://doi.org/10.1088/0031-8949/87/01/015201.
22. S. C. Pieper, K. Varga and R. B. Wiringa, *Quantum Monte Carlo calculations of A=9,10 nuclei*, Phys. Rev. C **66** (2002) 044310. https://doi.org/10.1103/PhysRevC.66.044310.
23. https://www.phy.anl.gov/theory/research/density/.
24. B. Buck, C. B. Dover and J. P. Vary, *Simple potential model for cluster states in light nuclei*, Phys. Rev. C **11** (1975) 1803. https://doi.org/10.1103/PhysRevC.11.1803.
25. I. Angeli and K. P. Marinova, *Table of experimental nuclear ground state charge radii: An update*, At. Data Nucl. Data Tables **99** (2013) 69-95. https://doi.org/10.1016/j.adt.2011.12.006.
26. C. Ngô, B. Tamain, M. Beiner, R. J. Lombard, D. Mas, H. H. Deubler, *Properties of heavy ion interaction potentials calculated in the energy density formalism*, Nucl. Phys. A **252** (1975) 237. https://doi.org/10.1016/0375-9474(75)90614-4.
27. H. Ngô and C. Ngô, *Calculation of the real part of the interaction potential between two heavy ions in the sudden approximation*, Nucl. Phys. A **348** (1980) 140-156. https://doi.org/10.1016/0375-9474(80)90550-3.
28. H. Schechter and L. F. Canto, *Proximity formulae for folding potentials*, Nucl. Phys. A **315** (1979) 470. https://doi.org/10.1016/0375-9474(79)90623-7.

29. R. K. Gupta, D. Singh and W. Greiner, *Semiclassical and microscopic calculations of the spin-orbit density part of the Skyrme nucleus-nucleus interaction potential with temperature effects included*, Phys. Rev. C **75** (2007) 024603. https://doi.org/10.1103/PhysRevC.75.024603.

30. S. Shlomo and J. B. Natowitz, *Temperature and mass dependence of level density parameter*, Phys. Rev. C **44** (1991) 2878. https://doi.org/10.1103/PhysRevC.44.2878.

31. J. Blocki, J. Randrup, W. J. Swiatecki and C. F. Tsang, Proximity forces, *Ann.Phys. (NY)* **105** (1977) 427. https://doi.org/10.1016/0003-4916(77)90249-4.

32. O. N. Ghodsi and R. Gharaei, *Temperature dependence of the repulsive core potential in heavy-ion fusion reactions*, Phys. Rev. C **85** (2012) 064620. https://doi.org/10.1103/PhysRevC.85.064620.

33. R. Gharaei and O. N. Ghodsi, *Role of Surface Energy Coefficients and Temperature in the Fusion Reactions Induced by Weakly Bound Projectiles*, Commun. Theor. Phys. **64** (2015) 185-196. https://doi.org/10.1088/0253-6102/64/2/185.

34. W. D. Myers and W. J. Swiatecki, *Nucleus-nucleus proximity potential and superheavy nuclei*, Phys. Rev. C **62** (2000) 044610. https://doi.org/10.1103/PhysRevC.62.044610.

35. I. Dutt and R. K. Puri, *Role of surface energy coefficients and nuclear surface diffuseness in the fusion of heavy-ions*, Phys. Rev. C **81** (2010) 047601. https://doi.org/10.1103/PhysRevC.81.047601.

36. I. Dutt and R. K. Puri, *Systematic study of the fusion barriers using different proximity-type potentials for N=Z colliding nuclei: New extensions*, Phys. Rev. C **81** (2010) 044615. https://doi.org/10.1103/PhysRevC.81.044615.

37. I. Dutt and R. K. Puri, *Comparison of different proximity potentials for asymmetric colliding nuclei*, Phys. Rev. C **81** (2010) 064609. https://doi.org/10.1103/PhysRevC.81.064609.

38. W. D. Myers and W. J. Swiatecki, *Nuclear masses and deformations*, Nucl. Phys. **81** (1966) 1-60. https://doi.org/10.1016/0029-5582(66)90639-0.

39. W. Reisdorf, *Heavy-ion reactions close to the Coulomb barrier*, J. Phys. G: Nucl. Part. Phys. **20** (1994) 1297. https://doi.org/10.1088/0954-3899/20/9/004.

40. L. Zhang, Y. Gao, H. Zheng, M. R. Huang and X. Liu, *Moments of the three-parameter Fermi distribution*, Mod. Phys. Lett. A **32** 1750195 (2017). https://doi.org/10.1142/S0217732317501954.

41. A. Winther, *Dissipation, polarization and fluctuation in grazing heavy-ion collisions and the boundary to the chaotic regime*, Nucl. Phys. A **594** (1995) 203-245. https://doi.org/10.1016/0375-9474(95)00374-A.

42. R. Bass, *Threshold and angular momentum limit in the complete fusion of heavy ions*, Phys. Lett. B **47** (1973) 139-142. https://doi.org/10.1016/0370-2693(73)90590-X.

43. R. Bass, *Fusion of heavy nuclei in a classical model*, Nucl. Phys. A **231** (1974) 45-63. https://doi.org/10.1016/0375-9474(74)90292-9.

44. R. Bass, *Nucleus-Nucleus Potential Deduced from Experimental Fusion Cross Sections*, Phys. Rev. Lett. **39** (1977) 265. https://doi.org/10.1103/PhysRevLett.39.265.

45. P. R. Christensen and A. Winther, *The evidence of the ion-ion potentials from heavy ion elastic scattering*, Phys. Lett. B **65** (1976) 19-22. https://doi.org/10.1016/0370-2693(76)90524-4.

46. R. Brockmann, *Relativistic Hartree-Fock description of nuclei*, Phys. Rev. C **18** (1978) 1510. https://doi.org/10.1103/PhysRevC.18.1510.

47. L. D. Miller and A. E. S. Green, *Relativistic Self-Consistent Meson Field Theory of Spherical Nuclei*, Phys. Rev. C **5** (1972) 241. https://doi.org/10.1103/PhysRevC.5.241.

48. R. Brockmann and W. Weise, *Spin-orbit coupling in a relativistic Hartree model for finite nuclei*, Phys. Rev. C **16** (1977) 1282. https://doi.org/10.1103/PhysRevC.16.1282.

49. P. G. Reinhard, *The relativistic mean-field description of nuclei and nuclear dynamics*, Rep. Prog. Phys. **52** (1989) 439. https://doi.org/10.1088/0034-4885/52/4/002.

50. H. Toki, Y. Sugahara, D. Hirata, I. Tanihata and B. Carlson, *Properties of nuclei far from the stability line in the relativistic hartree theory*, Nucl. Phys. A **524** (1991) 633. https://doi.org/10.1016/0375-9474(91)90266-9.

51. G. A. Lalazissis, J. König and P. Ring, *New parametrization for the Lagrangian density of relativistic mean field theory*, Phys. Rev. C **55** (1997) 540. https://doi.org/10.1103/PhysRevC.55.540.

52. G. Lalazissis, S. Karatzikos, R. Fossion, D. P. Arteaga, A. Afanasjev and P. Ring, *The effective force NL3 revisited*, Phys. Lett. B **671** (2009) 36-41. https://doi.org/10.1016/j.physletb.2008.11.070.

53. W. W. Daehnick, J. D. Childs and Z. Vrcelj, *Global optical model potential for elastic deuteron scattering from 12 to 90 MeV*, Phys. Rev. C **21** (1980) 2253. https://doi.org/10.1103/PhysRevC.21.2253.

54. https://www-nds.iaea.org/exfor/.

55. N. K. Timofeyuk, P. Descouvemont and I. J. Thompson, *Threshold effects in the* $^{27}P(\frac{3}{2}^+)\rightarrow\ ^{26}Si+p$ *and* $^{27}Mg(\frac{3}{2}^+)\rightarrow\ ^{26}Mg+n$ *mirror decays and the stellar reaction* $^{26}Si(p,\gamma)^{27}P$, Phys. Rev. C **78** (2008) 044323. https://doi.org/10.1103/PhysRevC.78.044323.